Numerical Prediction of Turbulent Flow over Surface-Mounted Ribs

R. W. Benodekar,* A. J. H. Goddard,† A. D. Gosman,† and R. I. Issa‡
Imperial College of Science and Technology, London, England

Turbulent flows over surface-mounted thin and thick ribs are investigated using a new computational method for incompressible recirculating flows. The method employs a differencing scheme which simultaneously satisfies the requirements of low numerical diffusion and positivity of coefficients. The effects of turbulence are modeled by a variant of the k-ϵ turbulence model incorporating curvature corrections. The governing equations are solved by an efficient pressure-implicit split-operator algorithm. The predictions are compared with experimental data and previous calculations. The present results compare satisfactorily with most of the measurements and show a definite improvement over previous results.

Nomenclature

A = finite difference coefficient
$c_1, c_2, c_\mu, \sigma_k, \sigma_\epsilon, \kappa$ = turbulence constants: 1.44, 1.92, 0.09, 1.0, $\kappa^2/[(c_2-c_1)c_\mu^{1/2}]$, 0.4187
C_p = static pressure coefficient
F = total flux coefficient
G = turbulent kinetic energy generation
h = rib height
H = summation operator
H_D = domain height
H_R = height of recirculation
k = kinetic energy of turbulence, also interpolation factor in skew differencing
L = convection coefficient
ℓ_m = mixing length
L_u, L_d = length of upstream and downstream computational boundaries, respectively
L_R = length of recirculation
n = coordinate normal to streamline
p = pressure
Pe = cell Peclet number
R_c = radius of curvature
S = source
S_{ns} = shear stress along streamline
t = rib thickness
u, v = mean velocity in x and y directions, respectively
u_s = mean velocity in streamline direction
u_i = mean velocity in x_i direction
x_i, x, y = Cartesian coordinates
$\Delta x, \Delta y$ = cell dimensions
γ = flux blending factor
Γ = exchange coefficient
δ = boundary-layer thickness
$\delta x, \delta y$ = grid spacings
δs = distance along streamline
Δ_i = difference operator
ϵ = dissipation of turbulent kinetic energy
Λ = diffusion coefficient
μ = viscosity
ρ = density
σ = Prandtl number
τ = shear stress
Φ = general dependent variable

Superscripts

$n, n+1$ = nth and $n+1$th iterations, respectively
u, v = u and v velocities
$(\ )^*, (\ )^{**}, (\ )^{***}$ = intermediate field values

Subscripts

BSHD = bounded skew hybrid differencing
BSUD = bounded skew upwind differencing
central = central differencing
eff = effective
HD = hybrid differencing
n,s,e,w = north, south, east, and west cell faces
P,N,S,E,W,SW, SE,NW,NE = main and surrounding grid locations
skew = skew differencing
t = turbulent
w', w'' = skew upstream locations of w
Φ = general dependent variable
∞ = freestream

Introduction

TURBULENT flow around bluff bodies forms an important group of separated flows occurring in many situations of practical interest. This class of flow has proved to be difficult to predict since it poses many problems for numerical methods and turbulence models because of the curved streamlines and steep velocity gradients surrounding the body. The present investigation is concerned with the prediction of the particular case of turbulent flow around two-dimensional surface-mounted ribs.

Many predictions of recirculating flows have been attempted in the past using the finite difference method of solution. In many cases, a form of central or upwind differencing, or hybrid thereof,[1] has been used to calculate the convective transport terms, and turbulence effects have been represented by the k-ϵ model. This approach has been found to underpredict the gross features of the recirculation zone[2,3] due in part to the false numerical diffusion associated with the upwinding of convective terms which results from nonalignment of the coordinate grid with the flow direction (see, for example, Refs. 4 and 5). However, the accuracy of such predictions also depends on the validity of the turbulence model and, in this respect, the standard k-ϵ model is believed to inadequately account for important strain effects such as those resulting from streamline curvature.[6] Many variants of

---

Received July 1, 1983; revision received April 3, 1984.

*Research Assistant, Department of Mechanical Engineering.

†Reader, Department of Mechanical Engineering.

‡Lecturer, Department of Mineral Resources Engineering.

this model have been proposed to represent this effect; however, in order to evaluate these variants, it is necessary to reduce the numerical diffusion to negligible levels. This could be achieved by using a sufficiently fine grid, but investigators[3] have demonstrated that the hybrid differencing (HD) scheme is impractically sluggish to refinement. Clearly this approach is expensive in two dimensions and would scarcely be feasible in three dimensions. An alternative approach is to use a "higher order" differencing scheme.

In the latter vein, schemes such as skew differencing[7] and quadratic upstream interpolation[8] have been developed and applied. However, these methods have been found to generate nonphysical oscillations or "wiggles," especially in the vicinity of steep gradients. These are a consequence of negative coefficients appearing in the difference equations, which sometimes also give rise to problems of numerical instability. A way around the overshoot problem is to employ a local blend of low- and high-order differencing schemes in just the right proportions to remove the extrema. The "flux corrected transport"[9] and FRAM[10] explicit time-marching methods are the outcome of this approach, however, these are costly when only the steady-state solution is of interest. Moreover, the negative coefficients are not entirely suppressed.

Lai and Gosman[11] have developed a flux-blending scheme which eliminates negative coefficients and can be applied to produce implicit and conservative discretized equations. This scheme has been employed by Lai and Gosman to produce a blend of the standard upwind and Raithby's skew differencing schemes to give the bounded skew upwind differencing (BSUD) scheme which uses the former component to ensure positivity while preserving the lower numerical diffusion of the latter as much as possible. The resulting coefficient matrix is unconditionally diagonally dominant and, therefore, presents no problems of instability. A variant of this scheme is used here.

The objective of the present investigation was to develop a prediction method for bluff-body flows which is more robust, accurate, and economical than its predecessors. The method was assessed by comparison with experimental data for the following two cases:

1) Flow over a surface-mounted square rib, as studied experimentally using laser-Doppler anemometry by Crabb et al.[17]

2) Flow over a surface-mounted thin rib, for which the pitot-tube measurements of Good and Joubert[18] are available.

The earlier predictions by Vasilić-Melling[2] using the HD scheme and standard k-ϵ turbulence model were in poor agreement with the experimental data; for example, the dimensions of the recirculation region were underpredicted by up to 30%. Durst and Rastogi[13] later obtained predictions using skew differencing on the momentum equations and the HD scheme on the k-ϵ set. The latter was tested in its standard form and also with the curvature corrections of Refs. 14 and 15. Durst and Rastogi concluded that the skew differencing scheme did not offer any advantage in accuracy over the HD scheme, because both required fine grids of around 57×34 before exhibiting sensitivity to the turbulence corrections. Although their predictions showed an improvement over the previous calculations of Ref. 2, the shape of the recirculation zone was not predicted correctly and they expressed concern about the computer time requirements.

Bergeles and Athanassiadis[16] obtained predictions for the flow over a square prism using the HD scheme and the standard k-ϵ turbulence model on a fine grid of 65×45. The overall features of the downstream bubble were predicted satisfactorily.

The present calculations are carried out using a skew scheme in conjunction with different versions of the k-ϵ turbulence model. The conventional methodology for solving the equations of motion expressed in terms of the primitive variables u, v, p has been replaced by the pressure-implicit split-operator (PISO) procedure recently developed at Imperial College.[12] The PISO procedure uses a two-stage predictor-corrector sequence, which, at each cycle of iteration satisfies the continuity and linearized momentum equations more closely than hitherto. As a consequence, it has improved the computational efficiency four- to fivefold.

Mathematical Model

Statement of the Governing Equations

The governing equations for steady-state turbulent flow can be written in Cartesian tensor notation as follows:

Continuity:

$$\frac{\partial u_i}{\partial x_i} = 0 \tag{1}$$

Momentum:

$$\frac{\partial \rho u_j u_i}{\partial x_j} = -\frac{\partial p}{\partial x_i} + \frac{\partial}{\partial x_i}\left[\mu_{\text{eff}}\left(\frac{\partial u_i}{\partial x_j} + \frac{\partial u_j}{\partial x_i}\right)\right] \tag{2}$$

Here the effective viscosity hypothesis has been used to represent the combined molecular and turbulent (Reynolds) stresses, where

$$\mu_{\text{eff}} = \mu + \mu_t \tag{3}$$

and μ and μ_t are laminar and turbulent viscosities, respectively.

Turbulence Model

The turbulent viscosity is determined from the values of the time-mean turbulence energy k and its dissipation rate ϵ according to

$$\mu_t = \rho c_\mu k^2/\epsilon \tag{4}$$

The equations for k and ϵ can be written as[19]:

$$\frac{\partial \rho u_j k}{\partial x_j} = \frac{\partial}{\partial x_j}\left(\frac{\mu_{\text{eff}}}{\sigma_k}\frac{\partial k}{\partial x_j}\right) + G - \rho\epsilon \tag{5}$$

$$\frac{\partial \rho u_j \epsilon}{\partial x_j} = \frac{\partial}{\partial x_j}\left(\frac{\mu_{\text{eff}}}{\sigma_\epsilon}\frac{\partial \epsilon}{\partial x_j}\right) + c_1\frac{\epsilon}{k}G - c_2\rho\frac{\epsilon^2}{k} \tag{6}$$

where

$$G = \mu_t \frac{\partial u_i}{\partial x_j}\left(\frac{\partial u_i}{\partial x_j} + \frac{\partial u_j}{\partial x_i}\right)$$

The values of the coefficients in these equations are given in the Nomenclature.

Boundary Conditions

The form of the calculation domain is shown in Fig. 1. The inlet boundary AB is located by trial and error sufficiently upstream of the obstacle so that its presence is not felt and the outlet is located sufficiently downstream of the point of reattachment. The lower boundary corresponds to the wind tunnel wall and the upper boundary corresponds to a wall or free boundary according to the case. The values of the various dimensions and boundary conditions are given for each case in Table 1.

No-slip boundary conditions are imposed along the walls, zero normal gradients at the outlet plane, and $u = u_\infty$, $v = 0$ are specified along the free boundary, where present. At the inlet plane AB, a one-seventh power-law boundary-layer profile for a smooth wall is imposed on axial velocity as in the measurements of Refs. 17 and 18. The k and ϵ inlet profiles appropriate for the turbulent boundary layer are estimated as follows, assuming local equilibrium of turbulence within the boundary layer[19]:

$$k=\tau/\rho c_\mu^{1/2} \tag{7}$$

$$\epsilon=k^{3/2}c_\mu^{3/4}/\ell_m \tag{8}$$

where, from the assumed stress strain hypotheses, τ is written as

$$\tau=\rho\ell_m^2\left(\frac{\partial u}{\partial y}\right)^2 \tag{9}$$

A ramp function distribution of ℓ_m is assumed. That is,

$$\begin{aligned}\ell_m &=\kappa y_P \quad &&\text{for } y_P\le c_\mu\delta/\kappa\\ &=c_\mu\delta \quad &&\text{for } y_P> c_\mu\delta/\kappa\end{aligned} \tag{10}$$

The freestream values of k and ϵ are estimated from the following relations:

$$k_\infty=0.0001u_\infty^2 \tag{11}$$

and

$$\epsilon_\infty=k_\infty^{3/2}c_\mu^{3/4}/(c_\mu\delta) \tag{12}$$

Near the wall, the Couette flow assumption of a constant shear stress is made. The standard log-law-based wall functions thus obtained for smooth wall and zero pressure gradients are used for the parallel velocity component and the turbulence quantities k and ϵ.[19] No attempt was made to take account of the adverse pressure gradients in the wall function formulations.

Turbulence Model Corrections

The two corrections to the k-ϵ model examined in Ref. 6 are used here in combination. One attempts to account for the effects of streamline curvature on c_μ in Eq. (4), thus,

$$c_\mu=\max\left\{0.025,\ \frac{0.09}{\left[1+0.57\frac{k^2}{\epsilon^2}\left(\frac{\partial u_s}{\partial n}+\frac{u_s}{R_c}\right)\frac{u_s}{R_c}\right]}\right\} \tag{13}$$

where u_s/R_c and $\partial u_s/\partial n$ are calculated by the procedure outlined in Ref. 6. The second modification, which was originally proposed by Hanjalić and Launder,[20] is aimed at simulating the preferential influence of normal stresses on the dissipation of turbulence energy by modifying the production term, $P\equiv\epsilon c_1 G/k$ in Eq. (6) to read:

$$P_\epsilon'=\frac{\epsilon}{k}\,[c_1'G-c_1''\mu_t S_{ns}^2] \tag{14}$$

where $c_1'=2.24$, $c_1''=0.8$ (giving $c_1'-c_1''=c_1$), and S_{ns} is calculated as in Ref. 6.

Discretization Scheme

General Finite Volume Equation

Figure 2 shows a control volume around a typical grid node P. The surrounding grid nodes are designated in compass fashion. The control volume faces are represented by the labels w, e, n, and s. The usual finite volume process of integrating Eqs. (2), (5), and (6) over the control volume at P and introducing suitable centered approximations for the diffusion terms yields:

$$L_w\Phi_w-L_e\Phi_e+L_s\Phi_s-L_n\Phi_n+\Lambda_e(\Phi_E-\Phi_P)-\Lambda_w(\Phi_P-\Phi_W)$$
$$+\Lambda_n(\Phi_N-\Phi_P)-\Lambda_s(\Phi_P-\Phi_S)-S_\Phi\Delta x\Delta y=0 \tag{15}$$

The BSHD scheme is used to approximate the convective fluxes [i.e., the first four terms on the left-hand side of Eq. (15)] as described below.

The BSHD Scheme

The BSHD scheme will be presented here for the case of a uniform grid for simplicity. As the name implies, it uses a hybrid method in approximating the convective fluxes in which the BSUD scheme[11] is used for $|Pe|>2$ and central differencing is invoked in the range of $|Pe|\le 2$, where the cell Peclet number Pe is defined as:

$$Pe=L/\Lambda \tag{16}$$

Expressions for the two approximations, for example, at the west face can be written as

$$(L_w\phi_w)_{\text{skew}}=L_w[P_w^u\Phi_{w'}+(1-P_w^u)\Phi_{w''}] \quad \text{for } |Pe_w|>2 \tag{17}$$

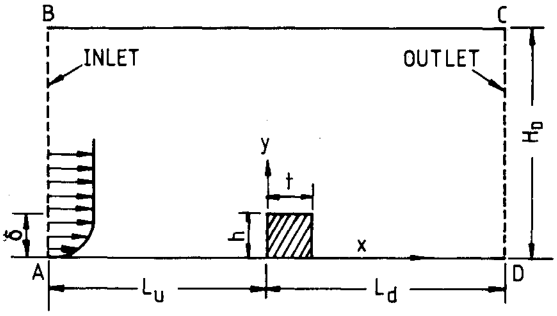

Fig. 1 The domain of calculation.

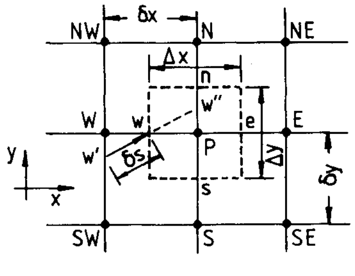

Fig. 2 Finite volume grid representation.

Table 1 Geometrical parameters

Parameter	Square rib[17]	Thin rib[18]
h, m	0.0235	0.1
H_D, m	0.3	1.0
t	h	$0.01h$[a]
L_u, m	$\ge 6h$	$\ge 6h$
L_d, m	$\ge 20h$	$\ge 20h$
δ	$0.5h$	$0.4h$
Top boundary	Wall	Free boundary
u_∞, m/s	18	26

[a] Good and Joubert[18] used a rib of thickness $0.04h$ and with a sharp tip formed by an inclined surface at the top. A rib of reduced thickness is simulated in an effort to approximate the sharp tip.

$$(L_w\phi_w)_{\mathrm{central}} = L_w\left(\frac{\Phi_W + \Phi_P}{2}\right) \quad \text{for } |Pe_w| \le 2 \tag{18}$$

where

$$P^u_w = \frac{1}{2}\left(1 + \frac{|u_w|}{u_w}\right) \tag{19}$$

It should be noted that ϕ_w is an approximation to Φ_w.

A discontinuity between Eqs. (17) and (18) at the transition Peclet number given by $|Pe_w| = 2$ gives rise to oscillations during iterative calculations. It is removed here by introducing the appropriate amount of diffusion in the right-hand side of Eq. (17), thus,

$$(L_w\phi_w)_{\mathrm{skew}} = L_w[P^u_w\Phi_{w'} + (1-P^u_w)\Phi_{w''}] + 2\Lambda_w\delta s\left(\frac{\partial\Phi}{\partial s}\right)_w \tag{20}$$

Here the extra diffusion term is equal to the first-order error term in the skew upwind approximation at $|Pe_w| = 2$. The total flux coefficient expressions for the west face can now be assembled as follows.

Central Differencing

$$F_{w,\mathrm{central}}/\Lambda_w = (\tfrac{1}{2}Pe_w + 1)\Phi_W + (\tfrac{1}{2}Pe_w - 1)\Phi_P \quad \text{for } |Pe_w| \le 2 \tag{21}$$

Skew Differencing

Here, for simplicity, we consider the case $u > 0$, $v > 0$, since the other velocity directions are treated similarly.

$$F_{w,\mathrm{skew}} = L_w\Phi_{w'} + 2\Lambda_w\delta s\left(\frac{\partial\Phi}{\partial s}\right)_w - \Lambda_w(\Phi_P - \Phi_W) \tag{22}$$

Substituting for $(\partial\Phi/\partial s)_w = (\Phi_w - \Phi_{w'})/\delta s$, $\Phi_w = (\Phi_P + \Phi_W)/2$, and $\Phi_{w'} = (1-k_w)\Phi_W + k_w\Phi_{SW'}$, where the linear interpolation factor k_w is given by[7]

$$k_w = \min\left(1, \ \frac{1}{2}\left|\frac{v_W}{u_w}\right| \left|\frac{\Delta x}{\delta y}\right|\right) \tag{23}$$

we get

$$\frac{F_{w,\mathrm{skew}}}{\Lambda_w} = Pe_w\Phi_W - (Pe_w - 2)k_w(\Phi_W - \Phi_{SW}) \quad \text{for } Pe_w > 2 \tag{24}$$

It can be easily verified that the two expressions given by Eqs. (21) and (24) are equal at $Pe_w = 2$. As will be shown below, when Eqs. (21) and (24) are substituted into Eq. (15), the resulting equation may have negative main coefficients (i.e., coefficients linking P to E,W,N,S), whereas the corner coefficients linking P to SW, SE, etc., are always positive. Following Lai and Gosman,[11] "flux blending" is used here to suppress the negative coefficients. The blend of skew differencing and the lower order HD scheme employed to produce the BSHD approximation can be represented as

$$F_{w,\mathrm{BSHD}} = \gamma_w F_{w,\mathrm{skew}} + (1-\gamma_w)F_{w,\mathrm{HD}} \quad \text{where } 0 \le \gamma \le 1 \tag{25}$$

It now follows that

$$F_{w,\mathrm{BSHD}}/\Lambda_w = Pe_w\Phi_W - (Pe_w - 2)\gamma_w k_w(\Phi_W - \Phi_{SW}) \tag{26}$$

as

$$F_{w,\mathrm{HD}}/\Lambda_w = Pe_w\Phi_W \tag{27}$$

We write similar total flux expressions for the remaining three faces of the cell and substitute these approximations in Eq. (15). By rearranging the terms and collecting the coefficients, the resulting equation can be cast into the following form:

$$A_P\Phi_P = A_N\Phi_N + A_S\Phi_S + A_E\Phi_E + A_W\Phi_W + A_{SW}\Phi_{SW} + A_{SE}\Phi_{SE} + A_{NW}\Phi_{NW} + A_{NE}\Phi_{NE} + S_P \tag{28}$$

where, for example, the W and SW coefficients are given by

$$A_W = [\{|L| - \gamma k(|L| - 2\Lambda)\}P^u]_w - \{\gamma k(|L| - 2\Lambda)P^u(1-P^v)\}_s - \{\gamma k(|L| - 2\Lambda)P^uP^v\}_n \tag{29}$$

and

$$A_{SW} = \{\gamma k(|L| - 2\Lambda)P^uP^v\}_w + \{\gamma k(|L| - 2\Lambda)P^uP^v\}_s \tag{30}$$

The above expressions are valid for all sign combinations of the u and v velocities. The suffixes written outside the brackets operate on all variables inside the brackets. Definitions similar to Eqs. (19) and (23) exist for P^u_n, P^u_s and k_n, k_s, respectively.

It is evident that the corner coefficients, which are in the form of Eq. (30), are always positive. Close inspection of A_W, however, shows that although the first square-bracketed term is always positive, the remaining two terms, which arise from flux contributions at the south and north faces of the cell, have a negative sign; thus, A_W could become negative. The flux-blending procedure of Ref. 11 evaluates the γ's in Eq. (29) such that $A_W \ge 0$. This is done by an optimization procedure which yields

$$\gamma_s = \min(\gamma_s^m, \ a/a_s)$$
$$\gamma_n = \max(0, \ (a - a_s\gamma_s)/a_n) \tag{31}$$

where

$$a = [\{|L| - k(|L| - 2\Lambda)\}P^u]_w$$
$$a_s = \{k(|L| - 2\Lambda)P^u(1-P^v)\}_s$$
$$a_n = \{k(|L| - 2\Lambda)P^uP^v\}_n \tag{32}$$

and the superscript m stands for the upper bound of γ. For $a_n > a_s$ relations (31) also apply, with subscripts s and n interchanged. The positivity of the remaining three main coefficients is checked in a similar way and the γ's are evaluated at all cell faces. Finally, the coefficients of Eq. (28) are assembled in a conservative manner.

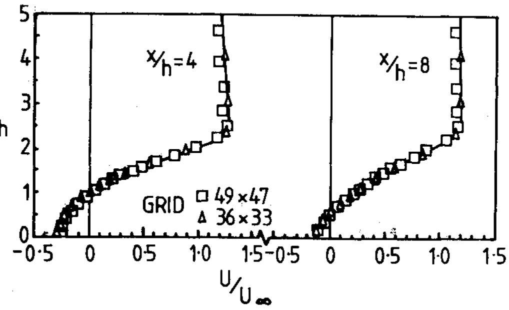

Fig. 3 Grid dependence of BSHD scheme with standard k-ϵ turbulence model for the square rib problem.

Solution Procedure

A staggered grid system is employed as in the TEACH code,[21] in which the velocity components are stored midway between the pressure storage locations. The present method of solution uses the PISO algorithm of Ref. 12, which is a two-stage predictor-corrector procedure. It involves the splitting of operations to deal with the coupling between velocity and pressure variables such that at each stage in the solution procedure, a set of equations in terms of a single unknown variable is obtained. This facilitates the use of standard methods for solving linear sets such as Eq. (28); for the present application a line successive overrelaxation scheme is employed.

The operation of PISO will now be outlined. Let the superscripts *, **, and *** denote intermediate field values obtained during the splitting process. The equations are factorized as follows:

1) Predictor step. The pressure field prevailing at the nth iteration is used in the solution of the implicit momentum equations given by Eq. (28) to yield the u_i^* velocity field. Thus,

$$A_P u_i^* = H(u_i^*) - \Delta_i p^n + S_i \tag{33}$$

where the operator H stands for $\Sigma A_m u_{i,m}$ in Eq. (28) (m is the grid node identifier and the summation is over the eight surrounding grid nodes) and Δ_i stands for the finite difference equivalent of grad. At this stage u_i^* and p^n satisfy momentum, but u_i^* does not satisfy continuity.

2) First corrector step. A new field u_i^{**}, together with a corresponding new pressure field p^*, is now sought such that the zero-divergence condition

$$\Delta_i u_i^{**} = 0 \tag{34}$$

is met. For this the operative momentum equation is written as:

$$A_P u_i^{**} = H(u_i^*) - \Delta_i p^* + S_i \tag{35}$$

However, for simplicity (see Ref. 12), an incremental form of the momentum equation is derived by subtracting Eq. (33) from Eq. (35) to obtain

$$A_P (u_i^{**} - u_i^*) = -\Delta_i (p^* - p^n) \tag{36}$$

When Eq. (36) is substituted into relation (34), the following pressure increment equation is obtained:

$$\Delta_i [A_P^{-1} \Delta_i] (p^* - p^n) = \Delta_i u_i^* \tag{37}$$

Equation (37) is solved for the $(p^* - p^n)$ field, which is then inserted into Eq. (36) to get the new velocity field u_i^{**}. These fields, it can be shown, do not satisfy the (linearized) momentum equations to an acceptably accurate degree; hence, the second corrector step.

3) Second corrector step. A new velocity field u_i^{***}, together with its corresponding field p^{**}, is formulated so that

$$\Delta_i u_i^{***} = 0 \tag{38}$$

The operative momentum equation is now taken as

$$A_P u_i^{***} = H(u_i^{**}) - \Delta_i p^{**} + S_i \tag{39}$$

Subtracting Eq. (35) from Eq. (39) gives

$$A_P (u_i^{***} - u_i^{**}) = H(u_i^{**} - u_i^*) - \Delta_i (p^{**} - p^*) \tag{40}$$

This equation, combined with the continuity relations (38) and (34), yields the pressure increment equation

$$\Delta_i [A_P^{-1} \Delta_i] (p^{**} - p^*) = \Delta_i [A_P^{-1} H(u_i^{**} - u_i^*)] \tag{41}$$

Equation (41) is solved for the $(p^{**} - p^*)$ field, which is then used in conjunction with Eq. (40) to obtain u_i^{***}. This completes the splitting process at which stage the u_i^{***} and p^{**} fields are taken to stand for the $(n+1)$th iteration values, u_i^{n+1} and p^{n+1}. It is theoretically proven in Ref. 12 that the fields obtained thus are very close approximations to the true solution of the linear discretized equations [Eqs. (33-41)]. In particular, the pressure field p^{**} is based (as it should be) on a divergence-free velocity field u_i^{**}. It is this feature which

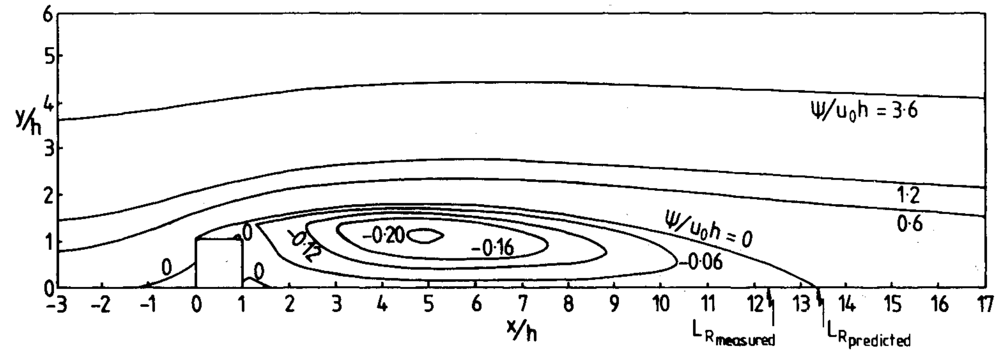

Fig. 4 Predicted streamlines for flow over the square rib.

Table 2 Computed values of L_R and H_R for flow over a thin rib

	Standard k-ϵ model							
	HD scheme		BSHD scheme		BSHD with modified k-ϵ model		Measurements of Good and Joubert[18]	
Grid	L_R/h	H_R/h	L_R/h	H_R/h	L_R/h	H_R/h	L_R/h	H_R/h
24×18	8.70	1.35	9.80	1.38				
36×33	9.72	1.55	11.29	1.67	12.76	1.78	13.2	2.16
49×47	10.12	1.70	11.50	1.76				

endows the overall algorithm with good stability and rapid convergence. The k and ϵ equations are solved next.

The above procedure is repeated in the given sequence until convergence is obtained; this is determined by examining the level or residual errors in each of the equation sets solved.

Results of Computations

Square Rib

The computations for the square rib correspond to the measurements of Crabb et al.[17] The grid distribution used for the predictions is similar to one used in Ref. 13 except that the grid is contracted and then expanded near the experimentally measured reattachment point instead of uniformly expanding downstream.

Two different grids were employed and representative results using the standard k-ϵ turbulence model are presented in Fig. 3 in the form of axial velocity profiles at two locations. It is seen that the solution for the 36×33 grid is to all intents and purposes grid-independent.

The calculated streamlines obtained with the turbulence model corrections incorporated are presented in Fig. 4. The predicted reattachment length L_R is $13.3h$, which is about 8% higher than the measured value of $12.3h$. The predicted height of recirculation of $1.8h$ agrees well with the value inferred from Crabb's data. The predictions clearly show the presence of a small counterrotating eddy behind the obstacle as observed in the measurements. The earlier predictions[2,16] fail to show this eddy.

The u-velocity profiles at different axial locations are compared with the data in Figs. 5 and 6. The agreement is quite close at $x/h = -2$, 6, and 10. There is some discrepancy in the upstream and downstream regions close to the rib, i.e., at $x/h = -0.4$ and 1.5. At $x/h = 13$, the predicted profile shows a slower recovery than the measured profile as a consequence of a longer reattachment length.

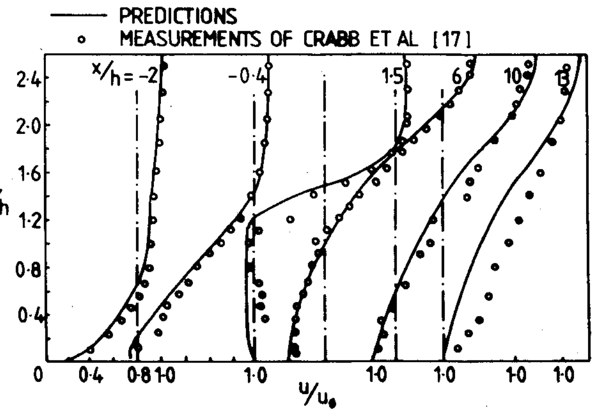

Fig. 5 Velocity predictions and measurements downstream of the square rib.

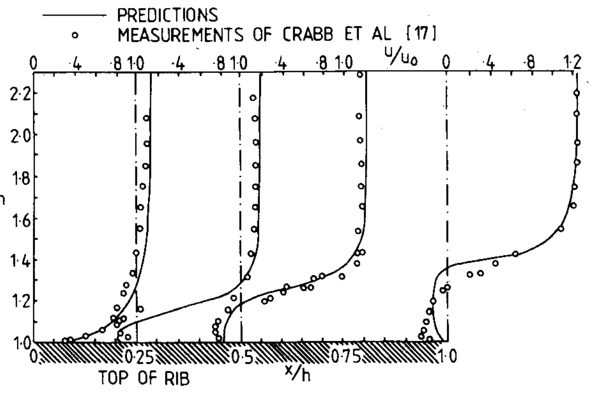

Fig. 6 Velocity predictions and measurements on top of the square rib.

The calculated wall static pressure distribution is compared with the measurements in Fig. 7. The correspondence is good upstream of the rib, but on the downstream side underprediction occurs for reasons which are not clearly understood. A similar discrepancy has been observed in Ref. 16. Nevertheless, the overall agreement is encouraging.

Thin Rib

This case is more difficult to predict than the previous one because of the singularity posed by the sharp tip of the fence. As noted earlier, this feature is approximated herein by making the computational rib thinner than the real one: it is represented by a single row of cells and the calculation domain upstream and downstream is covered by an expanding and contracting grid as used for the square rib problem.

Three substantially different grids were employed and the predicted values of L_R and the height of recirculation H_R are summarized in Table 2 for various combinations of differencing schemes and k-ϵ model variants. It is seen that L_R increases with the successive refinement of the grid and moves toward the measured value of $13.2h$.

It is clear from these results that the HD solutions change very slowly with grid refinement and independence is not established even for a mesh as fine as 49×47. On the other hand, the BSHD scheme shows an improvement of L_R of 10% over the HD results and shows signs of grid independence for the 49×47 mesh. In fact, the result with the 36×33 arrangement is only 2% below that of the finest grid.

The turbulence model corrections as described earlier were employed for the grid distribution of 36×33 and resulted in even closer correspondence with the measurements. This can be seen in Table 2 where predicted L_R is only 3.3% in error. Further evidence is presented in Figs. 8 and 9 showing the streamlines and velocity profiles generated using the 36×33 gird. The stream function contours of Fig. 8 show that the overall features of the downstream bubble are qualitatively well predicted but the quantitative discrepancy still remains with respect to the length and height of recirculation and the maximum negative value of the stream function. The comparison of velocity profiles in Fig. 9 shows excellent agreement outside the recirculation zone, but less satisfactory results within it. The latter discrepancies may be due to some extent to measurement errors as the pitot tube is unreliable in this region. In addition, as mentioned earlier, the sharp-edged inclined top used in measurements was not simulated exactly in the calculations. In this connection, Durst and Rastogi[13] observed in their experiments an increase of one rib height in L_R produced by making the edge sharp. Finally, inadequacies in the turbulence model and the wall function treatment based on the standard log law cannot be ruled out.

The predicted wall static pressure distribution is compared with the measurements in Fig. 10. As in the previous case, agreement is good in the region upstream of the rib, but discrepancies exist in the downstream region where the predicted profile shows faster recovery than the measurements.

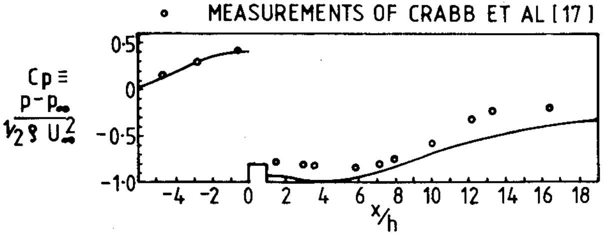

Fig. 7 Wall static pressure distribution for flow over the square rib.

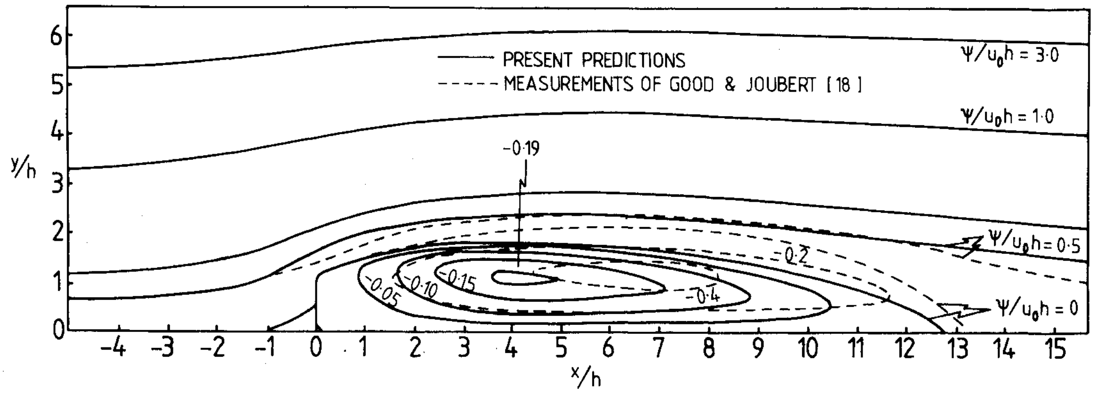

Fig. 8 Predicted streamlines and measurements for flow over the thin rib.

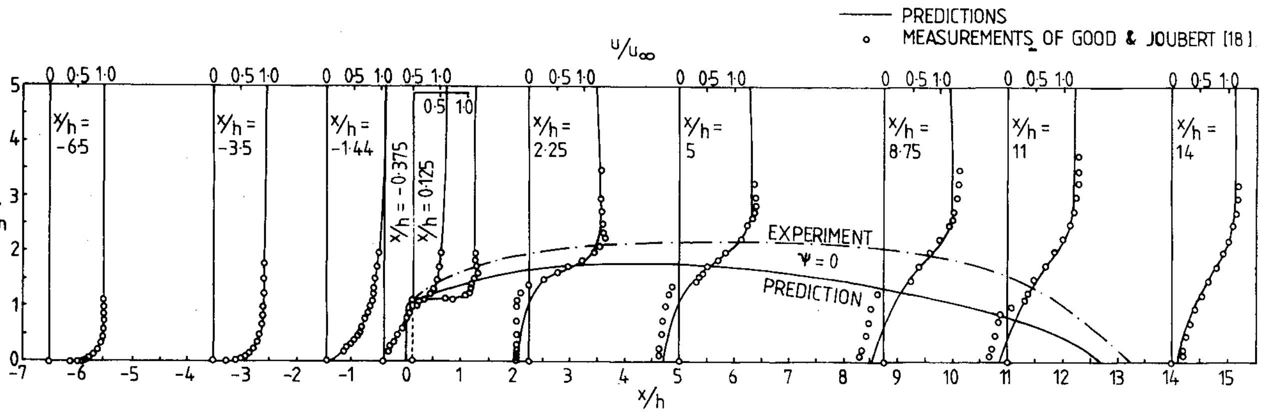

Fig. 9 Velocity predictions and measurements for flow over the thin rib.

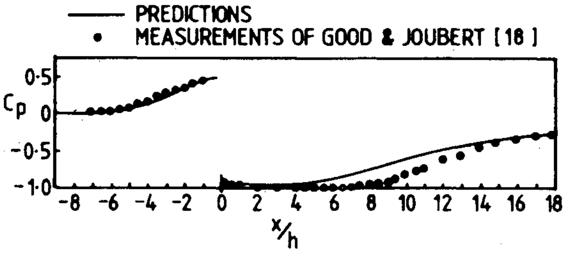

Fig. 10 Wall static pressure distribution for flow over the thin rib.

Table 3 Computing times for thin rib problem

Grid	Scheme	No. of iterations	CPU time, min
36×33	BSHD/SIMPLE	2200	46
36×33	BSHD/PISO	380	9
49×47	HD/SIMPLE	3600	102
49×47	HD/PISO	600	22

However, ultimately the two profiles recover to the same value at $x/h = 16$.

Comments on Cost Effectiveness

Table 3 summarizes the number of iterations and computing times (on an IBM 360/195 machine) required to obtain the solutions just presented. Also given are the figures obtained when the well-known SIMPLE[22] algorithm embodied in the original TEACH code was used instead of PISO. Two clear lessons emerge from the table: first, when it is borne in mind that the 36×33 BSHD solutions were appreciably more accurate than those of the HD scheme, it is clear that a substantial saving in CPU time has been achieved; second, further substantial improvement has resulted from the replacement of SIMPLE by PISO. Therefore, overall, the new methodology is substantially more cost-effective than that which it replaces.

Concluding Remarks

The combination of the BHSD scheme with its improved accuracy and the efficient PISO algorithm has resulted in a predictive method which is accurate, economical, and robust. When applied in conjunction with the corrections to the k-ϵ model of turbulence, it has resulted in improved predictions for the present applications.

The predictions for the square rib problem agree closely with the LDA measurements, which are believed to be reliable. The disagreement between the predicted and measured wall static pressure distributions cannot be explained.

The thin rib predictions agree qualitatively well with the measurements. The qualitative discrepancies are attributed to the sharp edge of the rib which is not exactly simulated in the predictions, turbulence model inadequacies, and, to some extent, errors in the measurements. Further research in the development and testing of turbulence models for the class of flow discussed here and more reliable measurements for the thin rib problem are desirable.

Acknowledgment

The support of this work by the Commission of the European Communities under Contract SR-016-UK(N) is gratefully acknowledged.

References

[1] Spalding, D. B., "A Novel Difference Formula for Differential Expressions Involving Both First and Second Derivatives," *International Journal for Numerical Methods in Engineering*, Vol. 4, 1972, pp. 334-338.

[2] Vasilić-Melling, D., "Three-Dimensional Turbulent Flow Past Rectangular Bluff Bodies," Ph.D. Thesis, Imperial College, London, 1976.

[3] McGuirk, J. J., Taylor, A. M. K. P., and Whitelaw, J. H., "The Assessment of Numerical Diffusion in Upwind-Differencing Calculations of Turbulent Recirculating Flows," Turbulent Shear Flows 3, Selected Papers from the 3rd Symposium on Turbulent Shear Flows, University of California, Davis, Sept. 1981, pp. 206-229.

[4] Raithby, G. D., "A Critical Evaluation of Upstream Differencing Applied to Problems Involving Fluid Flow," *Computer Methods in Applied Mechanics and Engineering*, Vol. 9, 1976, pp. 75-103.

[5] Castro, I. P., Cliffe, K. A., and Norgett, M. J., "Numerical Predictions of the Laminar Flow over a Normal Flat Plate," Theoretical Physics Division, Atomic Energy Research Establishment, Harwell, England, Rept. HL. 81/666, 1981.

[6] Leschziner, M. A. and Rodi, W., "Calculation of Annular and Twin Parallel Jets using Various Discretization Schemes and Turbulence-Model Variations," *Transactions of ASME*, Vol. 103, June 1981, pp. 352-360.

[7] Raithby, G. D., "Skew Upstream Differencing for Problems Involving Fluid Flow," *Computer Methods in Applied Mechanics and Engineering*, Vol. 9, 1976, pp. 153-164.

[8] Leonard, B. P., "A Stable and Accurate Convective Modeling Procedure Based on Quadratic Upstream Interpolation," *Computer Methods in Applied Mechanics and Engineering*, Vol. 19, 1979, pp. 59-98.

[9] Book, D. L., Boris, J. P., and Zalesak, S. T., "Flux-Corrected Transport," *Finite-Difference Techniques for Vectorized Fluid Dynamics Calculations*, edited by D. L. Book, Springer-Verlag, 1981, pp. 29-41.

[10] Chapman, M., "FRAM—Nonlinear Damping Algorithms for the Continuity Equation," *Journal of Computational Physics*, Vol. 44, No. 1, Nov. 1981, pp. 84-103.

[11] Lai, K. Y. M. and Gosman, A. D., "Finite-Difference and Other Approximations for the Transport and Navier Stokes Equations," Mechanical Engineering Department, Imperial College, London, Rept. FS/82/16, July 1982.

[12] Issa, R. I., "Solution of Implicitly Discretized Fluid Flow Equations by Operator-Splitting," Internal Report, Department of Mineral Resources Engineering, Imperial College, London, 1982; also, to be published in *Journal of Computational Physics*, 1985.

[13] Durst, F. and Rastogi, K., "Turbulent Flow Over Two-Dimensional Fences," *Proceedings of the 2nd Symposium on Turbulent Shear Flows*, Imperial College, London, July 1979, pp. 16.30-16.38.

[14] Militzer, J., Nicoll, W. B., and Alpay, S. A., "Some Observations on the Numerical Calculation of the Recirculation Region of Twin Parallel Symmetric Jet Flow," *Proceedings of the 1st Symposium on Turbulent Shear Flows*, University Park, Pa., Vol. 1, April 1977, p. 18.11.

[15] Launder, B. E., Priddin, C. H., and Sharma, B. I., "The Calculation of Turbulent Boundary Layers on Spinning and Curved Surfaces," *Journal of Fluids Engineering*, Vol. 99, No. 1, March 1977, pp. 231-239.

[16] Bergeles, G. and Athanassiadis, N., "Numerical Study of the Flow Around a Surface Mounted Prism," *Proceedings of Symposium on Refined Modelling of Flows*, Paris, Vol. 1, 1982, pp. 47-58.

[17] Crabb, D., Durao, D. F. G., and Whitelaw, J. H., "Velocity Characteristics in the Vicinity of a Two Dimensional Rib," *Proceedings of the 4th Brazilian Congress on Mechanical Engineering*, Florianopolis, Brazil, Dec. 1977, pp. 415-429.

[18] Good, M. C. and Jouber, P. N., "The Form Drag of Two-Dimensional Bluff Plates Immersed in the Turbulent Boundary Layers," *Journal of Fluid Mechanics*, Vol. 31, Feb. 1968, pp. 547-582.

[19] Launder, B. E. and Spalding, D. B., "The Numerical Computation of Turbulent Flows," *Computer Methods in Applied Mechanics and Engineering*, Vol. 3, 1974, pp. 269-289.

[20] Hanjalić, K. and Launder, B. E., "Preferential Spectral Transport by Irrotational Staining," *Proceedings of the 2nd Symposium on Turbulent Shear Flows*, Imperial College, London, 1979, pp. 10.37-10.42.

[21] Gosman, A. D. and Ideriah, F. J. K., "A General Computer Program for Two-Dimensional Turbulent Recirculating Flows," Department of Mechanical Engineering, Imperial College, London, Internal Report, June 1976.

[22] Patankar, S. V. and Spalding, D. B., "A Calculation Procedure for Heat, Mass and Momentum Transfer in Three-Dimensional Parabolic Flows," *International Journal of Heat and Mass Transfer*, Vol. 15, Oct. 1972, pp. 1787-1806.